




## Independent control method for plasmonic skin depth based on transformation from spoof surface plasmon polaritons to bound states in the continuum

Go Itami \* and Osamu Sakai *Department of Electronic Systems Engineering, The University of Shiga Prefecture, 2500 Hassaka-cho, Hikone, Shiga 522-8533, Japan* (Received 24 August 2022; revised 10 November 2022; accepted 21 November 2022; published 6 December 2022)

A metal plate array (MPA) is the complementary structure of a metal hole array and forms spoof surface plasmon polaritons (SSPPs) supported by parallel plate modes in a unit cell. A ring dipole array, which is a periodic structure designed by providing an aperture in the conductive part of the unit cell of an MPA, has the potential to produce bound states in the continuum (BICs). In this paper, the transformation from SSPPs to BICs is confirmed using these two structures by broadening the aperture in the unit cell. Making use of this phenomenon, control of the skin depth of surface modes is numerically demonstrated while retaining the resonant frequency, and the fitting values of the plasmonic skin depth are in good agreement with theoretical values.

DOI: [10.1103/PhysRevB.106.245406](https://doi.org/10.1103/PhysRevB.106.245406)

### I. INTRODUCTION

Periodic structure has been studied as one of the most effective methods for controlling electromagnetic (EM) waves such as light and radio waves. In general, the propagation conditions of EM waves can be described with the use of Maxwell equations, and they are clarified by considering the specific physical conditions and relevant parameters such as frequency, wave number, polarization, medium constants of permittivity and permeability, and so on. Therefore, the behavior of the waves can be controlled by using periodic structures based on the Bloch/Floquet theorem; for example, the dispersion relation can be varied since periodic boundary conditions restrict the wave numbers [1]. On the other hand, modulation of features of the unit cell such as the size and shape of conductive nanoparticles causes a change of resonant modes on the structure. Thus, designing a model brings with it the possibility of EM phenomena. Namely, research into periodic structure has the potential of producing a lot of applications across several relevant fields such as optics [2] and antenna engineering [3].

Bound states in the continuum (BICs) are a kind of special physical phenomenon of spatially localized states with a corresponding eigenfrequency within the band of a continuous spectrum [4–15]. BICs were proposed in the field of quantum mechanics [4], and their mechanism has been studied through several approaches, such as by the detection of perfect reflectivity of Bloch modes [10], by the examination of polarization of radiation [5], and by the disappearance of the resonance mode in the reflectance characteristics [11]. Since BICs can be specified by the characteristic divergence of their quality factor (Q-factor), this phenomenon has the potential for application to numerous systems in different fields, such as optical lasers [12], sensing devices [13], and antennas [14]. In recent work, it has been revealed that a toroidal dipole supported in

plasmonic chains can excite BICs; the resonant mode can be described by using a torus model of current distributions, and the applications of the model to metasurfaces have also been reported [8,9,15].

Metamaterial is also included in periodic structure and has variable potential of breaking through the physical limitations of natural materials [16–30]. For example, their typical features include a negative refractive index [16–18], a near-zero index [19], cloaking, and so on. The structures for the formation of the specific phenomena can be designed from two points of view such that resonator design is considered in the microscopic perspective and dispersion relation is mainly determined in the macroscopic perspective. Spoof surface plasmon polaritons (SSPPs) are metamaterial configurations covered by a broader definition [20–30]. SSPPs are like surface plasmon polaritons (SPPs) in that the behavior of the periodic EM modes that occur on its structure can be described in the same way as that of free electrons on the conductive surface of SPPs [31]. Since the modes in SSPPs are determined by structural parameters, the behavior of wave propagations can be controlled by using SSPP structures. The typical structure for generating SSPPs is a metal hole array (MHA), which is a two-dimensional conductive structure with periodic perforations [20,21,24–28,30]. The MHA is well-known as a structure for producing extraordinary transmissions proposed by Ebbesen *et al.* [27]. In general, just like MHAs, SSPP structures have been designed using an approach whereby a unit cell is made and arranged periodically in a conductive plate by cutting or making holes. However, in recent work, SSPP modes have also been confirmed in metal plate arrays (MPAs), which are a complimentary structure of MHAs, during the process of examining the breakdown of Babinet's principle [28]. Furthermore, since MPAs can also be regarded as plasmonic periodic structures, they are considered to be deeply related to BICs.

One of the applications of periodic structure is skin depth engineering which has been mainly studied recently in optical bands [32–34]. Skin depth engineering is expected to be used

\*ot68gitami@ec.usp.ac.jp

for the suppression of crosstalk and the reduction of energy loss in photonic devices. The proposed methods in these studies are varied, involving the use of dielectric metamaterials, composite metamaterials of dielectric and conductive structures, and others. In plasmonic bands, the skin depth control of SSPPs is also important, and some work has been done on this [21,29,30]. Firstly, the skin depth is numerically estimated by EM analyses [21,29], and the theoretical values are validated experimentally [30]. However, since the skin depth of SSPPs directly depends on dispersion relations and resonant modes, its control independent from other parameters such as resonant frequency is difficult in principle. Even if introduced as challenging technologies, independent control is expected to solve several problems in different fields, such as medical imaging and high-frequency circuits [35,36], and has potential for improving sensing technologies in terms of spatial resolution and multidimensionalization.

In this paper, an independent control method for plasmonic skin depth based on transformation from SSPPs to BICs is proposed. A ring dipole array (RDA), which is a perforated structure of an MPA, is used, and transformation of the surface modes from SSPPs to BICs by broadening the holes is confirmed with a resulting dramatic rise in the Q-factor. Since current distributions in a unit cell of an RDA can be modeled the same way as those in a toroidal dipole, an RDA is also considered to be able to form BICs [9]. In the corresponding BIC model, since the mode formation is independent of apertures in the unit cell, a drastic improvement in the Q-factor must be confirmed under the conditions of a fixed resonant frequency. On the other hand, from the viewpoint of SSPP formation, only the cutoff frequency is varied while retaining the resonant frequency because the mode is determined by the entire size of the conductive part in the unit cell. According to the theoretical definition of plasmonic skin depth, the value is determined only by the two frequencies, and the variance of the skin depth independent of the resonant frequency is demonstrated based on the above hypotheses.

In the following section, the wave propagation models in an RDA are described based on the mode formation of SSPPs and BICs. Next, the variance of the Q-factor of the RDA in the process of the transformation is discussed. Finally, a demonstration of a plasmonic skin depth independent of resonant frequency is reported in the case of the RDA.

## II. WAVE PROPAGATION THEOREM ON AN RDA

In this paper, the SSPP-to-BIC transformation phenomenon is discussed, and its application to a control method for plasmonic skin depth is demonstrated. This discussion of the phenomenon is started by providing an MPA for SSPP formation [28], as shown in Fig. 1(a). The size of the conductive part of the unit cell is  $a \times a \times w$ , and the period of the arrangements is  $d$ . An RDA, which is a perforated MPA, shown in Fig. 1(b), is also provided for BIC excitation. The size of the holes in the RDA is  $p \times p \times w$ . As Fig. 1(c) shows, SSPPs are excited on the MPA by incident waves at an optimal frequency, and the modes are considered to be transformed to BICs if the holes are made in the unit cell and  $p$  in the RDA

is increased, as shown in Fig. 1(d). The RDA is considered to form current distributions like those of a toroidal dipole which has been shown to excite BICs [8,9]. On the other hand, the RDA is also a perforated structure of an MPA, which is a complementary structure to an MHA, which is known to excite SSPPs. SSPP formation has already been confirmed in the case of MPAs as well as MHAs [28]. Making holes on each unit cell of an MPA gives different boundary conditions from that of SSPPs since the RDA structure can also be treated as a toroidal dipole with a BIC structure. First, a theoretical discussion of BIC formation on an RDA is presented based on toroidal dipole resonance in plasmonic nanoparticle chains. Next, SSPP formation on an MPA is described based on the wave propagation theorem in periodic structures, and finally, the connection between the transformation from SSPPs to BICs and skin depth control of surface modes on the structures is revealed.

BIC formation in the RDA can be described based on a similar model to the symmetric mode of a plasmonic nanoparticles chain with dominant toroidal dipole resonance [8,9,15]. The RDA is also considered to form electric (blue lines) and magnetic (red lines) circular currents between adjacent rings and around each ring in the unit cell, as shown in Fig. 1(d). These mode generations are obvious when electric and magnetic distributions are considered in the RDA. Since the fundamental mode of electric fields is formed in the gap between the adjacent rings, magnetic fields perpendicular to the electric fields are consequently formed. Namely, the two current distributions should be created due to the absence of energy leakage in the system. The top view of the mode in Fig. 1(d) is shown in Fig. 1(e). Since the mode in Fig. 1(e) has the complementary mode in Fig. 1(f), the observed mode is estimated as the synthesized mode shown in Fig. 1(g). In the synthesized mode, although the electric modes are canceled out, the modes should again form such that the magnetic mode responds. Only one of the modes in Fig. 1(e) is considered in the following discussion for easy understanding of the mechanism. As well as the symmetric mode of a plasmonic nanoparticles chain with dominant toroidal dipole resonance [9], the multiple-scattering theory is also considered based on the coupled dipole equation. Note that, since the formation of the plasmonic modes is the same as in the original model, a discussion of the mode formation is omitted. When a dynamic polarizability is  $\alpha(\omega) = (3i/2k_0^3)a_1$  and the relative permittivity of the metal is expressed as  $\epsilon(\omega) = 1 - \omega_p^2/\omega(\omega + i\gamma)$ , the coupled dipole equation can be expressed as follows. Here,  $a_1$  is the electric dipole term of the Mie coefficients [37,38],  $\omega_p$  is the plasma frequency, and  $\gamma$  is the collision frequency. However, no loss by collision is assumed in this model:

$$\mathbf{P}_m = \alpha(\omega) \left[ \mathbf{E}_{\text{ext}} + \sum_{n \neq m} \mathbf{g}(r_m - r_n) \mathbf{P}_n \right]. \quad (1)$$

Note that  $\mathbf{P}$  is the dipole moment of the nanoparticle, and  $\mathbf{g}(r)$  is the dyadic Green function. And the electric fields are assumed to form transverse-electric (TE) modes. Considering the similarity of the  $3 \times 3$  particles (A, B, C, D, E, F, G, H, and I) shown in Fig. 1(e) to the original model, the equation can be replaced as

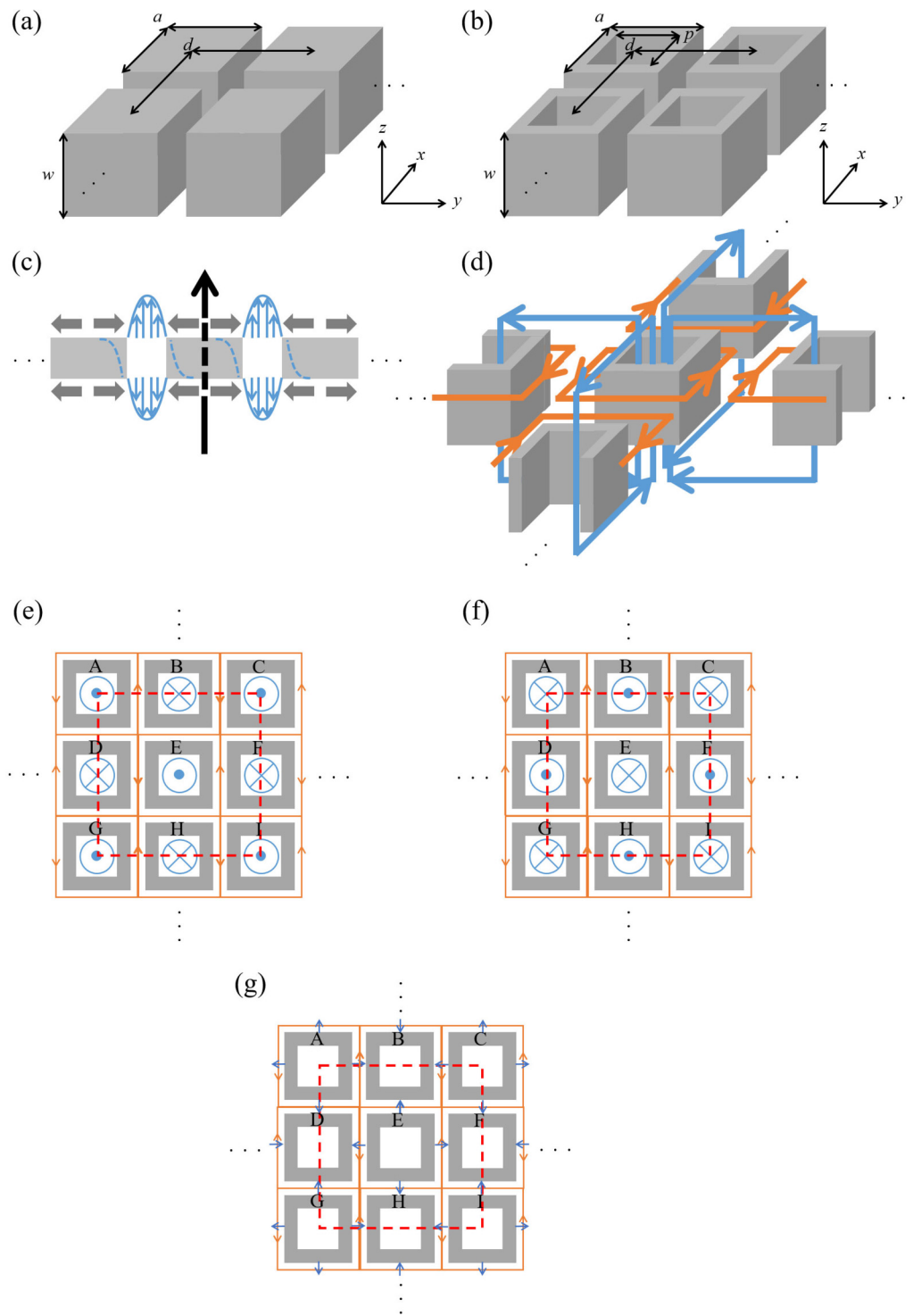


FIG. 1. Physical concept of converting propagation models on (a) a metal plate array and (b) a ring dipole array in accordance with the boundary shift from (c) a spoof surface plasmon polariton (SSPP) boundary to (d) a bound state in the continuum (BIC) boundary. The top views of (e) the mode of (d), (f) its complementary mode, and (g) the synthesized mode of (e) and (f). The blue and gray lines in (c) indicate electric modes and directions of SSPP oscillations. The blue and orange lines in (d)–(g) show directions of electric and magnetic modes. The red dashed lines in (e)–(g) express the unit cell of the BIC modes.

$$\begin{bmatrix} F(A) & -S_{AB} & -S_{AC} & -S_{AD} & -S_{AE} & -S_{AF} & -S_{AG} & -S_{AH} & -S_{AI} \\ -S_{BA} & F(B) & -S_{BC} & -S_{BD} & -S_{BE} & -S_{BF} & -S_{BG} & -S_{BH} & -S_{BI} \\ -S_{CA} & -S_{CB} & F(C) & -S_{CD} & -S_{CE} & -S_{CF} & -S_{CG} & -S_{CH} & -S_{CI} \\ -S_{DA} & -S_{DB} & -S_{DC} & F(D) & -S_{DE} & -S_{DF} & -S_{DG} & -S_{DH} & -S_{DI} \\ -S_{EA} & -S_{EB} & -S_{EC} & -S_{ED} & F(E) & -S_{EF} & -S_{EG} & -S_{EH} & -S_{EI} \\ -S_{FA} & -S_{FB} & -S_{FC} & -S_{FD} & -S_{FE} & F(F) & -S_{FG} & -S_{FH} & -S_{FI} \\ -S_{GA} & -S_{GB} & -S_{GC} & -S_{GD} & -S_{GE} & -S_{GF} & F(G) & -S_{GH} & -S_{GI} \\ -S_{HA} & -S_{HB} & -S_{HC} & -S_{HD} & -S_{HE} & -S_{HF} & -S_{HG} & F(H) & -S_{HI} \\ -S_{IA} & -S_{IB} & -S_{IC} & -S_{ID} & -S_{IE} & -S_{IF} & -S_{IG} & -S_{IH} & F(I) \end{bmatrix} \begin{bmatrix} P_A \\ P_B \\ P_C \\ P_D \\ P_E \\ P_F \\ P_G \\ P_H \\ P_I \end{bmatrix} = \begin{bmatrix} E_{\text{ext},A} \\ E_{\text{ext},B} \\ E_{\text{ext},C} \\ E_{\text{ext},D} \\ E_{\text{ext},E} \\ E_{\text{ext},F} \\ E_{\text{ext},G} \\ E_{\text{ext},H} \\ E_{\text{ext},I} \end{bmatrix}, \quad (2)$$

$$F(X) = \alpha_X^{-1} - S_X X, \quad X = A, B, \dots, I. \quad (3)$$

$$S_{AA} = S_{BB} = \dots = S_{II} = \sum_{n \neq 0} g(na) \exp(iqna), \quad (4)$$

$$S_{AB} = S_{BC} = \dots = S_{HI} = \sum_n g(na + d) \exp(iqna), \quad (5)$$

$$S_{AC} = S_{BD} = \dots = S_{GI} = \sum_n g(na + 2d) \exp(iqna), \quad (6)$$

$$S_{AD} = S_{BE} = \dots = S_{FI} = \sum_n g(na + 3d) \exp(iqna), \quad (7)$$

$$S_{AE} = S_{BF} = \dots = S_{EI} = \sum_n g(na + 4d) \exp(iqna), \quad (8)$$

$$S_{AF} = S_{BG} = \dots = S_{DI} = \sum_n g(na + 5d) \exp(iqna), \quad (9)$$

$$S_{AG} = S_{BH} = S_{CI} = \sum_n g(na + 6d) \exp(iqna), \quad (10)$$

$$S_{AH} = S_{BI} = \sum_n g(na + 7d) \exp(iqna), \quad (11)$$

$$S_{AI} = \sum_n g(na + 8d) \exp(iqna), \quad (12)$$

$$S_{BA} = S_{CB} = \dots = S_{IH} = \sum_n g(na - d) \exp(iqna), \quad (13)$$

$$S_{CA} = S_{DB} = \dots = S_{IG} = \sum_n g(na - 2d) \exp(iqna), \quad (14)$$

$$S_{DA} = S_{EB} = \dots = S_{IF} = \sum_n g(na - 3d) \exp(iqna), \quad (15)$$

$$S_{EA} = S_{FB} = \dots = S_{IE} = \sum_n g(na - 4d) \exp(iqna), \quad (16)$$

$$S_{FA} = S_{GB} = \dots = S_{ID} = \sum_n g(na - 5d) \exp(iqna), \quad (17)$$

$$S_{GA} = S_{HB} = S_{IC} = \sum_n g(na - 6d) \exp(iqna), \quad (18)$$

$$S_{HA} = S_{IB} = \sum_n g(na - 7d) \exp(iqna), \quad (19)$$

$$S_{IA} = \sum_n g(na - 8d) \exp(iqna). \quad (20)$$

Since all the particles in the RDA are the same size, the case of  $r_0 = r_1$  in Ref. [9] is assumed, and  $\alpha_A = \alpha_B = \alpha_C$ . To discuss BIC formation, the eigenequation of  $\mathbf{M}\mathbf{P} = \lambda\mathbf{P}$  is provided. Here, the inverse of the eigenvalue of  $1/\lambda_q(\omega)$  corresponds to the  $q$ th mode polarizability  $\alpha_q(\omega)$  of the plasmonic mode.

The dispersion relation of the plasmonic modes can be drawn by tracing the peak of  $\text{Im}[\alpha_q(\omega)]$ , and  $\text{Re}[\alpha_q(\omega)]$  takes zero when  $\text{Im}[\alpha_q(\omega)]$  is the peak in the Lorentzian-shape spectrum. Due to the equation of  $\text{Re}[\lambda_q(\omega)] = \text{Re}[\alpha_q(\omega)]/|\alpha_q(\omega)|^2$ , the dispersion relation can be obtained by solving the

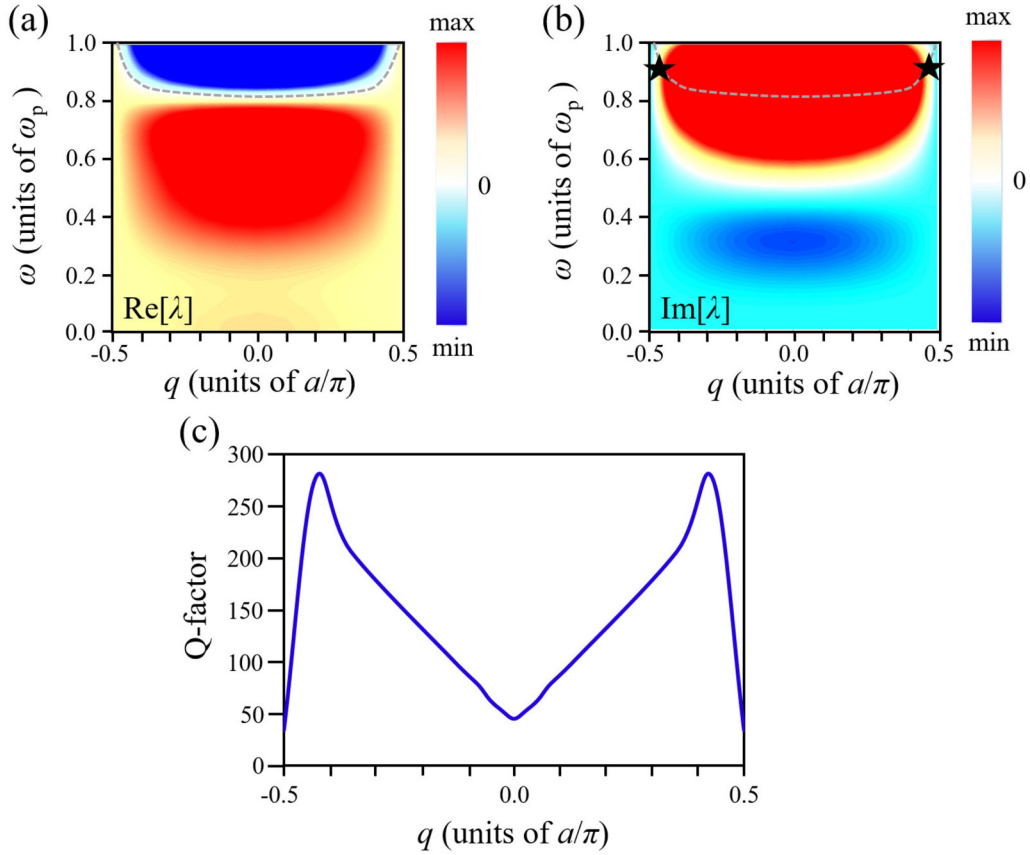


FIG. 2. (a) Real and (b) imaginary parts of eigenvalues of the plasmonic particle system for the ring dipole array (RDA), where gray dotted lines and two closed stars indicate boundary regions to zero and excited points of the bound state in the continuum (BIC) modes, respectively, and (c) the Q-factor characteristics of the RDA which is numerically analyzed using an electromagnetic simulator HFSS in the case of  $(a, d, p, w) = (2, 3, 1.6, 3 \text{ mm})$ .

equation of  $\text{Re}[\lambda_q(\omega)] = 0$ . In other words, the state corresponds to  $\mathbf{MP} = 0$ , and  $\alpha_q(\omega)$  is diverged, and therefore,  $\mathbf{P}$  represents a bound state. The eigenvalues of the plasmonic particle system and the characteristics of the Q-factor when  $d = 3 \text{ mm}$  and  $a = 2 \text{ mm}$  are shown in Fig. 2. Note that, as shown in Ref. [9], when considering the BICs at the  $\Gamma$  point, the zero-order factor in the subwavelength of  $u_0 = P_A \exp(iqd) + P_B + P_C \exp(-iqd)$  is related to the leak channel, if a one-dimensional model is assumed for the sake of simplicity. In Fig. 2, the results of (a) and (b) in a simplified three-body chain model show that there are two points of BIC formation. Since the plasmonic particles are the same size in this case ( $r_0 = 1.0r_1$ ), the results are in accordance with those of Ref. [9]. Furthermore, the result shown in Fig. 2(c) confirms that the characteristics of the Q-factor are consistent with the BIC formations derived by the values of  $\text{Re}[\lambda]$  and  $\text{Im}[\lambda]$ . Note that the characteristics are obtained by using an EM simulator HFSS (2021 R1, Ansys). The weak divergence of the Q-factor originates from the fact that the structural parameters are not optimized for only the BIC formations, whereas in this paper, we focus on the transformation from SSPPs to BICs. However, the result is reasonable because conventional studies for similar conductive and dielectric structures of at- $\Gamma$  and off- $\Gamma$  BICs also show the Q-factors  $\sim 200$  or  $< 200$  in simulated and experimental results [39,40]. Here, one of the similar points is that unit cells with finite size in the direction

perpendicular to the array direction are used. In the toroidal dipole model, since the size of an aperture in the conductive part of the unit cell is not directly influenced by the dispersion relation if the current distributions are conserved, the value of  $p$  is set to 1.6 mm for the optimization of the Q-factor. SSPPs were proposed by Pendry *et al.* [20] as plasmonic surface waves, and the dispersion relation of SSPPs is derived theoretically by using an MHA, which is a two-dimensional periodic structure of waveguides made of a conductive material. In the derivation, first, the TE incident waves are defined on the assumption of the existence of surface waves, and then the macroscopic relative permittivity and permeability are obtained by using the concept of average electric fields and the equation of energy flows in the boundary. Finally, the generation condition of SPPs and the values of macroscopic media are introduced into the wave equation at the boundary, and the dispersion relation is obtained. The formula is expressed as below:

$$\frac{\sqrt{k_{||}^2 - k_0^2}}{k_0} = \frac{S^2 k_0}{\sqrt{(\omega_p/c)^2 - k_0^2}}, \quad (21)$$

$$S^2 = \mu_x = \mu_y = \mu_m, \quad (22)$$

where  $k_0$  and  $k_{||}$  are wave numbers in free space and of surface modes, respectively,  $c$  is the velocity of light,  $S$  is the overlap

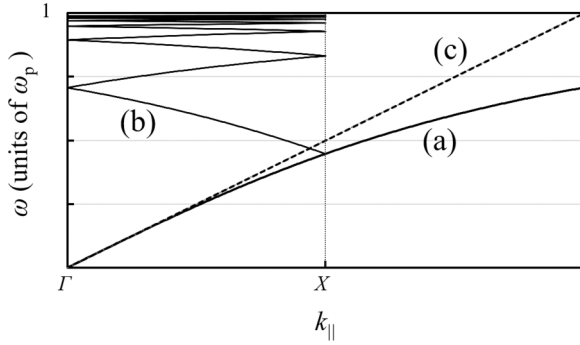


FIG. 3. Dispersion relation of (a) ideal and (b) real spoof surface plasmon polariton (SSPP) mode and (c) a light line in vacuum.

integral of the incident wave and the fundamental mode inside an SSPP resonator in the unit cell,  $\omega_p$  is a cutoff frequency, and  $\mu_m$  is the effective relative permeability in an SSPP structure [26].

Inversely, it can be said that any structure which satisfies the above EM conditions can also form SSPP modes even though the structure is different from an MHA. In fact, for example, SSPP formation has already been confirmed experimentally in the case of an MPA [28], which is a complementary structure of an MHA. In the case of the MPA, waves form parallel plate modes instead of waveguide modes in MHAs, and by considering the energy flow of the interval between the conductive parts at the boundary, the dispersion relation of the MPA can also be derived. Since the derivation process is like the original one, the basic configuration of the formula is not changed, but the parameters in regard to the effective media are replaced. Therefore,

$$S^2 = \frac{8a(d-a)}{\pi^2 d^2}, \quad \omega_p = \frac{\pi c}{a}. \quad (23)$$

Here, as well as SPPs, these curves do not directly intersect with a light line because of the differences of the phase velocities. However, in the case of SSPPs, lattice scattering effects within them have to be considered, and the effects enable the SSPP dispersion relations to couple with the light line. The effects are shown as follows:

$$k'_{||} = k_{||} \pm n|\mathbf{G}_x| \pm m|\mathbf{G}_y|, \\ |\mathbf{G}_x| = |\mathbf{G}_y| = \frac{2\pi}{d}. \quad (24)$$

Note that  $k'_{||}$  is the wave number of an SSPP with lattice scattering effects,  $|\mathbf{G}_x|$  and  $|\mathbf{G}_y|$  are the reciprocal lattice vectors in  $x$  and  $y$  directions, respectively. In fact, the effects are applied to the dispersion relations, and consequently, the curves show multiple higher modes in their characteristics. The curves are shown in Fig. 3, which confirms that the ideal curve of (a) does not intersect with the light line of (b); on the other hand, the real curve including the lattice scattering effects of (c) intersects the line. Based on the above SSPP theory, the plasmonic skin depth can be obtained with the following formula in the process of deriving the SSPP dispersion relation:

$$L = \frac{c}{\sqrt{\omega_p^2 - \omega_{\text{SSPP}}^2}}, \quad (25)$$

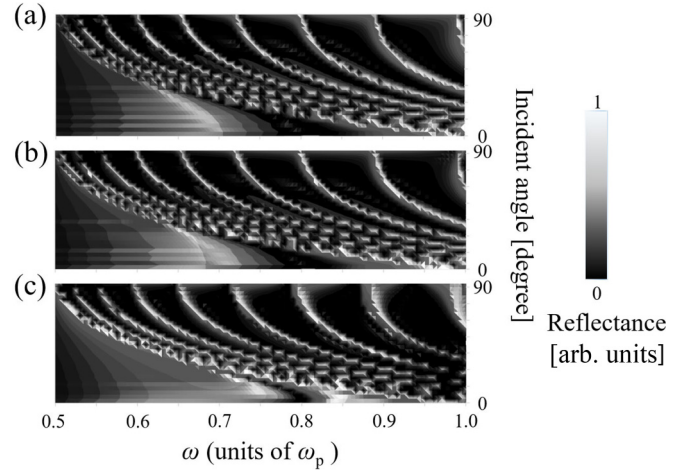


FIG. 4. Angular characteristics of the reflectance in the ring dipole array when (a)  $p = 0.2$  mm, (b)  $p = 1.0$  mm, and (c)  $p = 1.6$  mm.

where  $\omega_{\text{SSPP}}$  is the resonant frequency of the SSPP. From this equation, the plasmonic skin depth is determined only by the resonant frequency and the cutoff frequency [29,30]. In other words, the skin depth can be controlled while retaining the resonant frequency by just independently varying the cutoff frequency. If we use only SSPP modes, it is difficult to control the cutoff frequency or the resonant frequency independently by modifying the structure design because the surface modes are influenced simultaneously by both wave propagation effects, such as boundary conditions, and circuit effects, such as inductances and capacitances. However, if an aperture is set in the unit cell of an MPA, the cutoff frequency can be varied independently since the resonant mode is fixed by utilizing the process of transformation to BICs. Therefore, the plasmonic skin depth is considered to be controlled while retaining the resonant frequency.

### III. RESULTS AND DISCUSSIONS OF PLASMONIC SKIN DEPTH CONTROL USING A RDA

In this section, the various propagation characteristics on the RDA are discussed, and the control method for plasmonic skin depth is demonstrated numerically. In the analyses, an EM simulator HFSS is used for the examinations. First, the standard size of the RDA is defined as  $(a, d, p, w) = (2, 3, 1, 3$  mm) throughout the examinations. The value of  $w$  is fixed at 3 mm throughout the evaluations to keep the same conditions for surface mode formations. In the formations of both modes of SSPPs and BICs, the transverse-magnetic (TM) incidence is assumed as well as SPPs although microscopic electric distributions on the boundary in the unit cell represent TE modes, as discussed in the previous section [26,28]. Also, an infinite periodic boundary condition is applied to the RDA in the analyses. Figure 4 shows the dependencies of the incident angle of the reflective characteristics with the variance of  $p$ . As the entire tendency of all the results, the position of each intersection point changes continuously as the angle of incidence changes, which is consistent with the behavior of the theoretical curve since multiple discrete intersections with the light

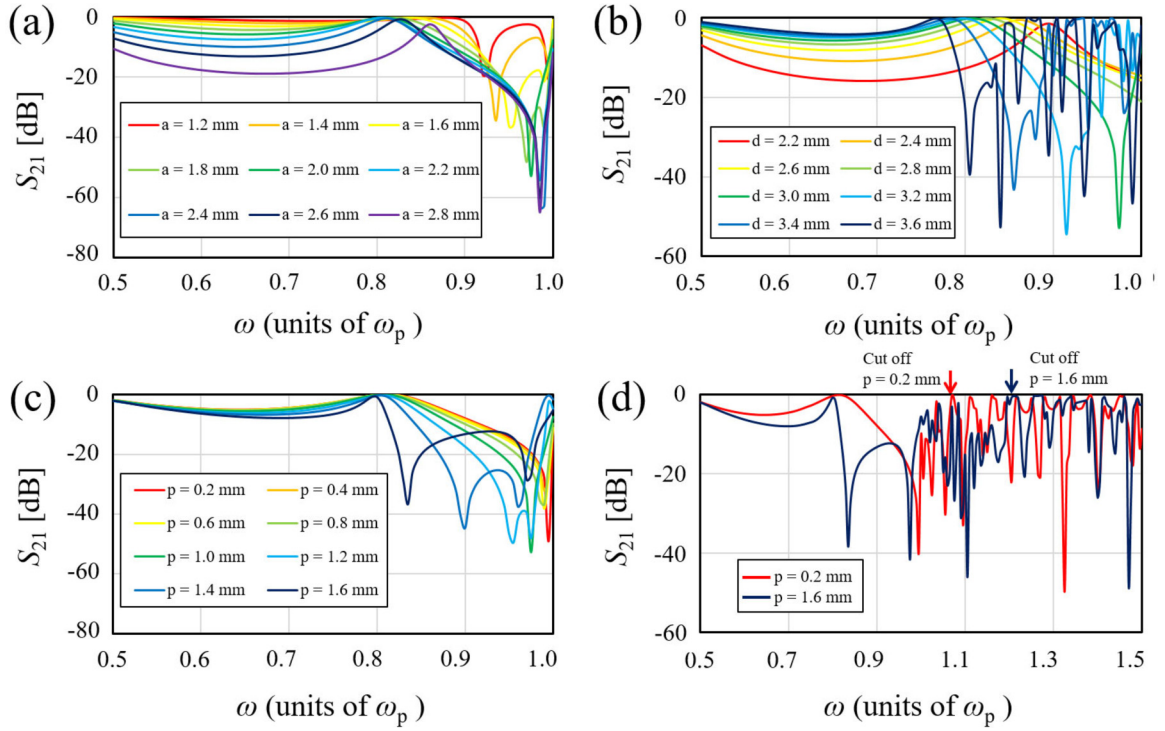


FIG. 5. The structural parameter dependencies of the transparent characteristics of the ring dipole array for different values of (a)  $a$ , (b)  $d$ , (c)  $p$ , and (d) the comparison results of the cutoff frequency when  $p = 0.2$  and  $1.6$  mm in (c).

line are generated if the incident angle is changed, as shown in Fig. 3. The sharpness of the peaks of each reflective mode is reduced as the value of  $p$  is increased. This is considered to be caused by being outside of SSPP modes. Furthermore, this confirms the decrease in the number of reflective modes with an increase in the value of  $p$ . This is because the reflective spectra are dulled in this situation. Also, viewing the overall tendency, the regions which show higher reflective intensity become larger as the value of  $p$  is increased. This change shows that the electric distribution on the structure approaches the BIC mode. The direction of the aftermath seeping out from each reflective mode changes between the cases of  $p = 0.2$  and  $1.6$  mm. This clearly indicates a qualitative change in the mode being formed. It is a conversion process from SSPPs to BICs and can be viewed as an unstable propagation state in terms of SSPP mode formation. As described in Ref. [28], the mode formation principle is strictly different between the pure SSPP case and the present case. In fact, the number of modes increases discontinuously from the case  $p = 0$  (Ref. [28]) to  $p = 0.2$  mm. This also supports the proposal of the mode generation based on the transformation from SSPPs to BICs.

Figure 5 shows the variations of the transmission characteristics on the RDA depending on the parameters of  $a$ ,  $d$ , and  $p$ . Here, the band pass frequency is the frequency which takes the first local maximum, and band stop frequency is defined as the points that take local minimum values. The cutoff frequency shows the point which takes the second local maximum of  $\sim 0$  dB as well as band pass frequency. In Fig. 5(a), as the value of  $a$  is increased, a band stop effect dominates below  $a = 2.2$  mm, while the band pass effect dominates above  $a = 2.2$  mm. This indicates the switch of the pattern of resonance modes formation. When  $a$  is relatively

small, the ring resonator acts mainly as a ring resonator, and when  $a$  is relatively large, the capacitance effect generated inside the ring becomes nonnegligible relative to the inductance, forming a resonance loop and generating a band pass effect. When  $a$  becomes even larger than that, it is clear that the SSPP mode is formed since the function as the boundary of the parallel plate mode becomes dominant rather than the inductance effect. Note that these processes do not eliminate the effect as a ring resonator. In Fig. 5(b), it is shown that the resonant frequency becomes lower as  $d$  is increased. In the case that SSPP modes are formed, the resonant frequency is dominated by the variation with  $d$ . This is evident from the fact that the SSPP dispersion relation in Fig. 3(b) is greatly affected by lattice scattering effects, and the lattice constant is a function of  $d$ . As  $d$  increases, the wave number at the  $X$  point decreases and the intersection with the light line (the resonance point) decreases. In Fig. 5(c), when  $p$  is large, the band stop resonance frequency becomes lower, while the band pass resonance frequency remains almost unchanged. The band stop resonant frequency is considered to decrease due to the improved inductance of the ring resonator. As discussed theoretically above, this consistency in the band pass resonance frequency is considered to occur in the process of the mode transformation from SSPPs to BICs. When  $p$  is sufficiently small, assuming the SSPP mode is like the MPA, it can be considered that the vertically incident radio wave and the SSPP dispersion relation are coupled, and the corresponding resonance frequency can be estimated to be  $\sim 0.8\omega_p$ , as shown in a previous study [28]. On the other hand, since the zero point for  $q = 0$  in BIC is also  $0.8\omega_p$ , as shown in Fig. 2(a), this is consistent with the view that SSPP formation in that frequency change does not occur during the conversion

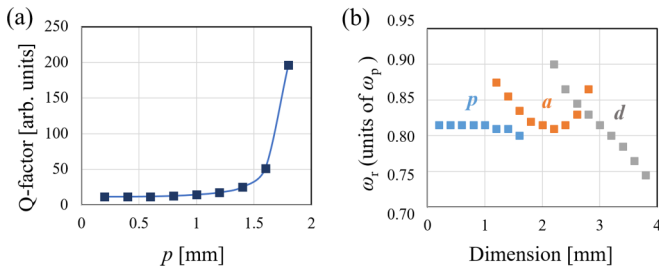


FIG. 6. (a) The  $p$  dependency of the Q-factor of the ring dipole array (RDA) and (b) the parameter dependencies of the resonant frequency of the RDA in the cases of  $a$ ,  $d$ , and  $p$ .

process to BIC since the frequencies of the two are identical. Figure 5(d) shows the comparison of the cutoff frequencies for the two values of  $p = 0.2$  and  $1.6$  mm. The cutoff frequency is higher for  $p = 1.6$  mm than for  $p = 0.2$  mm. The size of the outside of the ring is considered to determine the cutoff frequency: for small values of  $p$ , the ring conductor acts sufficiently as a ground, but for larger values of  $p$ , the inductance component becomes nonnegligible, resulting in a higher cutoff frequency. Therefore, band pass frequency does not depend on the EM circuit theory, while band stop frequency and cutoff frequency are based on the theory. To discuss the mode conversion from SSPPs to BICs, the Q-factor of the band pass frequency of RDA is considered in the following. Figure 6(a) shows a dramatic increase in the Q-factor when  $p$  is increased, as does Fig. 5(c). This increase is likely to coincide with the results of the off- $\Gamma$  mode in similar studies [39,40]. As discussed above, this is considered to be a characteristic of the conversion from SSPP mode to BIC mode when  $p$  is increased. Figure 6(b) shows the change in resonance frequency when each parameter is changed. Here,  $p$  shows only 1.9% change, which is quantitatively confirmed to be almost unchanged. Similarly, for  $a$  and  $d$ , the rates of change are 7.7 and 18.8%, respectively, and this also quantitatively confirms that the resonance frequency changes significantly, as in the SSPP structure. From the above discussion, by changing  $p$  in the RDA, the cutoff frequency can be varied while the resonance frequency is almost fixed. In other words, this

means that the plasmonic skin depth determined from these two frequencies can be changed while retaining the resonance frequency.

Next, the examination of the method for controlling plasmonic skin depth is discussed, based on the numerical demonstration results. First, the changes of the electric distributions around the RDA are confirmed by changing  $p$  from 0.4 to 1.4 mm. The results are shown in Figs. 7(a)–7(c). Note that the incident direction is from the bottom to the top side, and the waves are entered at the resonant frequency of  $0.8\omega_p$ . The overall tendency is for the electric distribution above the unit cell to become intensified as  $p$  is increased. The results also confirm that the electric fields are concentrated on the intervals of the adjacent unit cells, and the fields are not formed effectively inside the ring regardless of the value of  $p$ . These phenomena are consistent with the fact that the fundamental modes which the propagating waves form are located in the intervals of the adjacent unit cells, and the other higher modes are not produced [28]. In all the cases in Fig. 7, the concentrated electric fields are formed in such a way that they diffuse around the ring edge. In the cases of (a) and (b), as they differ from that of (c), the fields are considered to be different from simple near fields phenomenologically since there is almost no electric field concentration at the inner ring edges. In other words, it is just the result of the formation of surface modes on a macroscopic medium supported by periodic structures. Figures 7(d) and 7(e) show the electric and magnetic field distributions at the resonant frequency. Note that the incident directions of the electric and magnetic fields are horizontal and vertical directions, respectively. As discussed regarding the BIC mode generation using Fig. 1, the magnetic fields in (e)–(g) show the rotation around the ring, and the electric fields in (d) are canceled out inside the ring, and they oscillate along the horizontal direction between the adjacent rings. Next, the plasmonic skin depth control of surface modes generated near the RDA is described. In the propagation space shown in Fig. 7, the spatial distribution of the average electric field intensity on the opposite side of the incident plane was obtained. Figure 8 compares the results of the spatial distribution when  $p$  is varied as in the case shown in Fig. 7. The spatial distribution is calculated

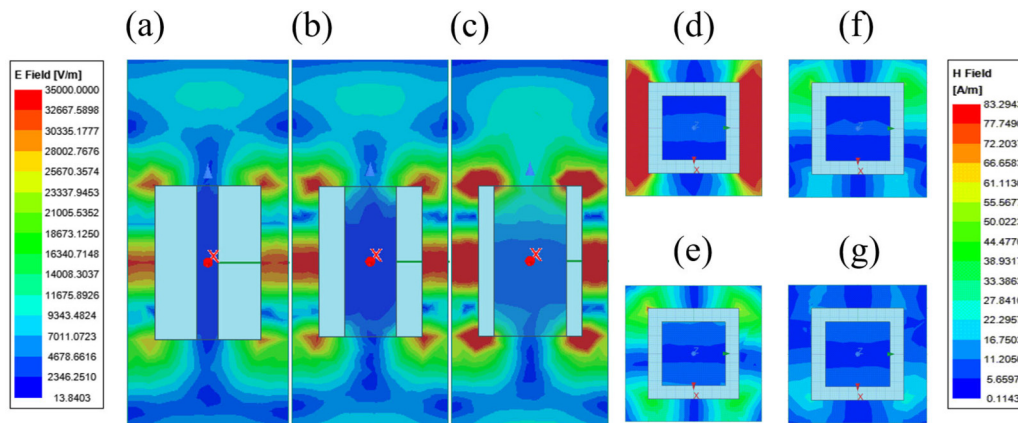


FIG. 7. The electric distributions around the ring dipole array when (a)  $p = 0.4$  mm, (b)  $p = 1.0$  mm, and (c)  $p = 1.4$  mm when viewed from the side. The top view of the (d) electric and (e) magnetic field distributions when  $p = 1.4$  mm. (f) and (g) are the distributions when the phase is advanced by  $60^\circ$  and  $120^\circ$  from the case of (e), respectively. All distributions are formed at the resonant frequency.



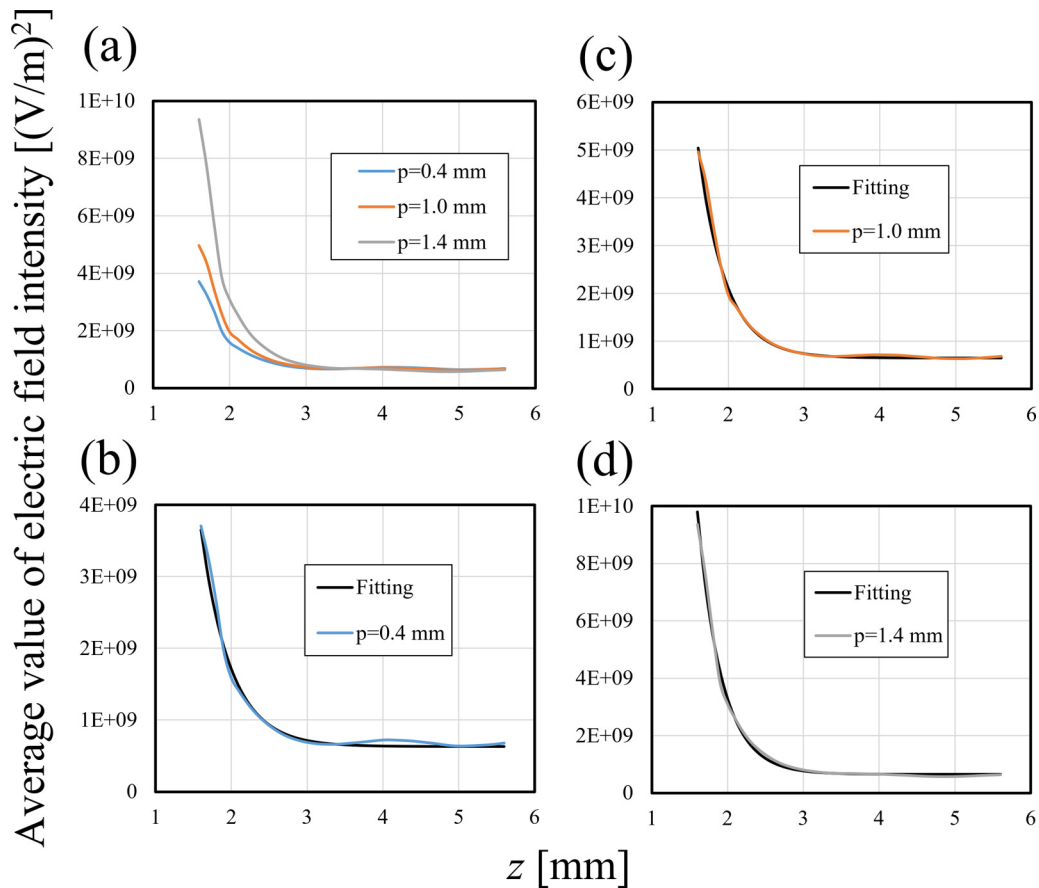


FIG. 8. The comparison results of (a) the spatial distributions of the electric field intensities when  $p = 0.4, 1.0,$  and  $1.4$  mm and between the distributions of (b)  $p = 0.4$  mm, (c)  $p = 1.0$  mm, and (d)  $p = 1.4$  mm and their fitting curves.

as a one-dimensional distribution in the  $z$  direction averaged from the electric field intensity in the  $x$ - $y$  plane. As shown in Fig. 8(a), all the spatial distributions exhibit exponential attenuation characteristics, with the maximum value of the field intensity increasing as the value of  $p$  increases. At the same time, the attenuation in the  $z$  direction also shows steeper characteristics. In other words, the plasmonic skin depth is indeed changing as the value of  $p$  is varied. The graphs of (b)–(d) in Fig. 8 show the results of exponential fitting of the spatial distribution of electric field intensity for each value of  $p$ . The fitting curve function is as follows:  $f(z) = A\exp[-(z - z_0)/(L_{\text{fit}}/2)] + B$ , and the values of each parameter are shown in Table I. Note that the spatial distributions have the square order of the electric fields. The spatial distribution of field intensity in (b)–(d) is in good agreement with the corresponding fitting curves. From Table I, as  $p$  increases, the skin depth

$L_{\text{fit}}$  decreases. On the other hand, as discussed in the previous section, Fig. 5(d) shows that the cutoff frequency  $\omega_p$  increases as  $p$  increases. From this fact and the theoretical equation (the formula of  $L$ ), the skin depth  $L$  decreases as  $p$  increases if the resonant frequency is fixed. Therefore, the results shown in Fig. 8 and Table I are indeed consistent with the theorem. Furthermore, using the propagation characteristics of the RDA and the theoretical equation for  $L$ , the estimated values of the plasmonic skin depth are obtained theoretically. As shown in Table I, the theoretically estimated values of the skin depth  $L_{\text{th}}$  at  $p = 0.4, 1.0,$  and  $1.4$  mm are  $0.69, 0.68,$  and  $0.54$  mm, respectively. The estimated values are in good agreement with the corresponding fitting values  $L_{\text{fit}}$  with errors of 13, 6, and 19%, respectively.

#### IV. CONCLUSIONS

Focusing on the SSPP mode formation in the MPA, which is a complementary structure of MHA, a control method for plasmonic skin depth is proposed, with the use of RDAs that have the perforated structures of MPAs, and its feasibility verified. The method is based on the transformation process from SSPP to BIC mode in RDAs, and its dispersion relation is derived using a toroidal dipole model, which is consistent with the numerical results of  $Q$ -factors in RDAs.

The propagation characteristics in the RDA confirmed the qualitative change of the mode associated with the

TABLE I. The fitting parameters when  $p = 0.4, 1.0,$  and  $1.4$  mm and the theoretical estimated values of the plasmonic skin depth in these cases.

$p$ (mm)	$A$ ( $\text{V/m}^2$ )	$L_{\text{fit}}$ (mm)	$z_0$ (mm)	$B$ ( $\text{V/m}^2$ )	$L_{\text{th}}$ (mm)
0.4	$3.9 \times 10^9$	0.78	1.5	$6.3 \times 10^8$	0.69
1.0	$5.8 \times 10^9$	0.72	1.5	$6.5 \times 10^8$	0.68
1.4	$1.3 \times 10^{10}$	0.64	1.5	$6.5 \times 10^8$	0.54

transformation from SSPP to BIC mode. The behavior of the resonance point in the parameter variation characteristics is consistent with the propagation theorem.

The numerical demonstration confirmed that the one-dimensional spatial distribution of surface modes at the resonant frequency of the RDA can be controlled by the length  $p$  of a side of the aperture while keeping the resonant frequency fixed. The behavior of the skin depth during control was consistent with the propagation theory, and the order of

the theoretical values is in good agreement with the demonstrated results, with an average error of 13%.

#### ACKNOWLEDGMENTS

This paper was supported by a Grant-in-Aid for Scientific Research from the Japanese Ministry of Education, Culture, Sports, Science and Technology, Japan. (JSPS KAKENHI Grants No. 18H03690 and No. 22K18704).

- 
- [1] A. Ishimaru, *Electromagnetic Wave Propagation, Radiation, and Scattering: From Fundamentals to Applications*, 2nd ed. (Wiley-IEEE Press, New Jersey, 2017).
- [2] U. Leonhardt and T. Philbin, *Geometry and Light: The Science of Invisibility* (Dover Publications, New York, 2012).
- [3] J. Volakis, *Antenna Engineering Handbook*, 4th ed. (McGraw Hill, New York, 2007).
- [4] J. von Neumann and E. P. Wigner, *Phys. Z.* **30**, 465 (1929).
- [5] B. Zhen, C. W. Hsu, L. Lu, A. D. Stone, and M. Soljacic, *Phys. Rev. Lett.* **113**, 257401 (2014).
- [6] Q. Song, M. Zhao, L. Liu, J. Chai, G. He, H. Xiang, D. Han, and J. Zi, *Phys. Rev. A* **100**, 023810 (2019).
- [7] Q. Song, J. Hu, S. Dai, C. Zheng, D. Han, J. Zi, Z. Q. Zhang, and C. T. Chan, *Sci. Adv.* **6**, eabc1160 (2020).
- [8] Y. Wang, Z. Han, Y. Du, and J. Qin, *Nanophotonics* **10**, 1295 (2021).
- [9] M. Gong, P. Hu, Q. Song, H. Xiang, and D. Han, *Phys. Rev. A* **105**, 033504 (2022).
- [10] S. Dai, L. Liu, D. Han, and J. Zi, *Phys. Rev. B* **98**, 081405(R) (2018).
- [11] C. W. Hsu, B. Zhen, J. Lee, S. L. Chua, S. G. Johnson, J. D. Joannopoulos, and M. Soljčić, *Nature* **499**, 188 (2013).
- [12] C. Huang, C. Zhang, S. Xiao, Y. Wang, Y. Fan, Y. Liu, N. Zhang, G. Qu, H. Ji, J. Han *et al.*, *Science* **367**, 1018 (2020).
- [13] C. W. Hsu, B. Zhen, A. D. Stone, J. D. Joannopoulos, and M. Soljčić, *Nat. Rev. Mater.* **1**, 16048 (2016).
- [14] E. Melik-Gaykazyan, K. Koshelev, J. H. Choi, S. S. Kruk, A. Bogdanov, H. G. Park, and Y. Kivshar, *Nano Lett.* **21**, 1765 (2021).
- [15] Y. He, G. Guo, T. Feng, Y. Xu, and A. E. Miroshnichenko, *Phys. Rev. B* **98**, 161112(R) (2018).
- [16] J. B. Pendry, *Phys. Rev. Lett.* **85**, 3966 (2000).
- [17] R. A. Shelby, D. R. Smith, and S. Schultz, *Science* **292**, 77 (2001).
- [18] A. Sanada, C. Caloz, and T. Itoh, *IEEE Trans. Microwave Theory Tech.* **52**, 1252 (2004).
- [19] G. D'Aguanno, N. Mattiucci, M. J. Bloemer, R. Trimm, N. Aközbeke, and A. Alù, *Phys. Rev. B* **90**, 054202 (2014).
- [20] J. B. Pendry, L. M. Moreno, and F. J. G. Vidal, *Science* **305**, 847 (2004).
- [21] F. Miyamaru and M. Hangyo, *Phys. Rev. B* **71**, 165408 (2005).
- [22] S. A. Maier, S. R. Andrews, L. Martín-Moreno, and F. J. García-Vidal, *Phys. Rev. Lett.* **97**, 176805 (2006).
- [23] M. J. Lockyear, A. P. Hibbins, and J. R. Sambles, *Phys. Rev. Lett.* **102**, 073901 (2009).
- [24] J. Parsons, E. Hendry, C. P. Burrows, B. Auguie, J. R. Sambles, and W. L. Barnes, *Phys. Rev. B* **79**, 073412 (2009).
- [25] F. Miyamaru, M. Tanaka, and M. Hangyo, *Phys. Rev. B* **74**, 153416 (2006).
- [26] F. J. Garcia-Vidal, L. Martín Moreno, and J. B. Pendry, *J. Opt. A: Pure Appl. Opt.* **7**, S97 (2005).
- [27] T. W. Ebbesen, H. J. Lezac, H. F. Ghaemi, T. Thio, and P. A. Wolff, *Nature* **391**, 667 (1998).
- [28] G. Itami and O. Sakai, *Sci. Rep.* **10**, 11027 (2020).
- [29] O. Schnitzer, *Phys. Rev. B* **96**, 085424 (2017).
- [30] G. Itami and O. Sakai, *J. Appl. Phys.* **125**, 213101 (2019).
- [31] J. Katyal and R. K. Soni, *Plasmonics* **9**, 1171 (2014).
- [32] S. Jahani and Z. Jacob, *Nat. Nanotechnol.* **11**, 23 (2016).
- [33] A. Vora, J. Gwamuri, A. Kulkarni, J. M. Pearce, and D. O. Gunev, *Sci. Rep.* **4**, 4901 (2014).
- [34] T. Li, H. Liu, F. M. Wang, Z. G. Dong, and N. Zhu, *Opt. Express* **14**, 11155 (2006).
- [35] G. Itami, O. Sakai, and Y. Harada, *Electronics* **8**, 239 (2019).
- [36] A. Kianinejad, Z. N. Chen, and C. Qiu, *IEEE Trans. Microwave Theory Tech.* **64**, 3078 (2016).
- [37] O. Merchiers, F. Moreno, F. González, and J. M. Saiz, *Phys. Rev. A* **76**, 043834 (2007).
- [38] K. H. Fung and C. T. Chan, *Opt. Lett.* **32**, 973 (2007).
- [39] S. Sun, Y. Ding, H. Li, P. Hu, C. W. Cheng, Y. Sang, F. Cao, Y. Hu, A. Alù, D. Liu *et al.*, *Phys. Rev. B* **103**, 045416 (2021).
- [40] G. Yadav, S. Sahu, R. Kumar, and R. Jha, *Photonics* **9**, 292 (2022).